Journal of The Electrochemical Society, **156** (6) B716-B720 (2009)
0013-4651/2009/156(6)/B716/5/$25.00 © The Electrochemical Society

Ni/C Slurries Based on Molten Carbonates as a Fuel for Hybrid Direct Carbon Fuel Cells

Yuta Nabae,[a,c] Kevin D. Pointon,[b] and John T. S. Irvine[a,*,z]

[a]*School of Chemistry, University of St. Andrews, St. Andrews, Fife KY16 9ST, Scotland, United Kingdom*
[b]*Dstl Porton Down, Physical Sciences Department, Salisbury, Wiltshire SP4 0QR, United Kingdom*

Ni-impregnated carbon black (Ni/XC-72R) was tested as a fuel for a hybrid direct carbon fuel cell (HDCFC) with a hybrid electrolyte of yttria-stabilized zirconia and molten carbonate (Li_2CO_3/K_2CO_3). The open-circuit voltage (OCV) of the HDCFC with Ni/XC-72R was quite high, about 1.5 V at 700°C. The maximum power density was improved by factors of 7.6 and 3.1, respectively, at 550 and 700°C by adding 50 wt % of Ni catalyst. The effect of the Ni catalyst on the carbon/carbonate slurry was investigated by temperature-programmed decomposition. The Ni catalyst probably contributes to the high OCV by enhancing the reverse Boudouard reaction ($C + CO_2 \leftrightharpoons 2CO$) in the carbon/carbonate slurry in the HDCFC.
 [DOI: 10.1149/1.3110862]

Manuscript submitted October 1, 2008; revised manuscript received February 5, 2009. Published April 14, 2009.

The direct carbon fuel cell (DCFC) is a fuel cell that utilizes solid carbon directly as a fuel.[1] One significant advantage of this technology is the high energy density of solid carbon compared to that of alternative fuel sources such as hydrogen and methane both on a volumetric[2] and mass[3] density basis. Carbon fuels can be obtained from coal, cracking of hydrocarbons, or pyrolysis of biomass. Biomass is a very attractive energy source in terms of renewable energy.

Several concepts of DCFC have been demonstrated by employing conventional electrolyte materials such as molten hydroxide,[4] molten carbonate,[3,5-7] and solid oxide.[8-11] These DCFCs show promising open-circuit voltages (OCVs), but the current densities have not been enough to consider commercial applications, while the fuel cells based on hydrogen have received a great deal of attention. The difficulty in carbon oxidation in DCFCs relates to the nature of carbon. The reactivity and fluidity of solid carbon are lower than those of gaseous fuels such as hydrogen. Improving the anode kinetics is the key issue to achieve a high performance with DCFCs.

The HDCFC is a promising concept to improve the anode kinetics in DCFCs.[12,13] It merges the solid oxide fuel cell and molten carbonate fuel cell technologies. A solid oxide electrolyte is employed to separate the cathode and anode compartments, while a molten carbonate electrolyte is utilized in the anode compartment. Oxygen is reduced to O^{2-} at the cathode and transported across the solid electrolyte membrane to the carbon/carbonate slurry, where carbon is oxidized. Carbon is oxidized to CO and CO_2 in the anode compartment, with the selectivity dependent on temperature.

We demonstrated this concept using tubular[2,13] and small planar HDCFCs.[14] The tubular setup is suitable for practical demonstrations with some model fuels including biomass-based fuel, while the planar one was developed to investigate the anode reaction in detail. Previous works suggested that the addition of molten carbonate to the anode compartment drastically improved the anode kinetics of DCFC but the anode polarization was still limiting the DCFC performance. Further improvement of the anode kinetics is quite important to achieve a high performance with HDCFC.

This paper discusses the addition of a Ni catalyst on the carbon fuel with the purpose of improving the kinetics of carbon oxidation in HDCFCs. Ni nanoparticles were loaded on the carbon fuel by the conventional impregnation method and the Ni/carbon powder was tested as a fuel for the HDCFC.

Experimental

Ni impregnation.— The Ni catalyst loaded on carbon (Ni/XC-72R) was prepared by the conventional impregnation method. Carbon black (Cabot, XC-72R) was dispersed into an aqueous solution of $Ni(NO_3)_2 \cdot 6H_2O$. The mixture was stirred for several hours and then dried at 80°C. The powder of the catalyst precursor was reduced with H_2 (5%, balanced with Ar) for 5 h at 400°C.

Electrochemical measurement.— The details of the test cell used in this study are described in a previous paper.[14] A NiO/yttria-stabilized zirconia (YSZ) anode and a $(La_{0.8}Sr_{0.2})_{0.95}MnO_3$ (LSM)/YSZ composite cathode were applied on opposite surfaces of a YSZ pellet (2 mm thickness and 20 mm diameter) by screen printing. The anode and cathode were sintered at 1300 and 1250°C, respectively. The geometric surface area of the electrodes was 1.13 cm^2.

Figure 1 shows a schematic diagram of the test cell. Gold meshes and gold wires were attached to the pellet using gold paste (Metalor Technologies T10112) for current collection. The pellet was attached to an alumina tube with a ceramic paste (Aremco 668). The electrochemical oxidation of Ni/XC-72R was carried out under batch fuel conditions in this study. A eutectic mixture of 62 mol % Li_2CO_3 (Sigma-Aldrich) and 38 mol % K_2CO_3 (Fisher) was mixed with Ni/XC-72R [carbon/carbonate (1:1 mol)] and put into the cell at room temperature. The standard amount of the carbon fuel was

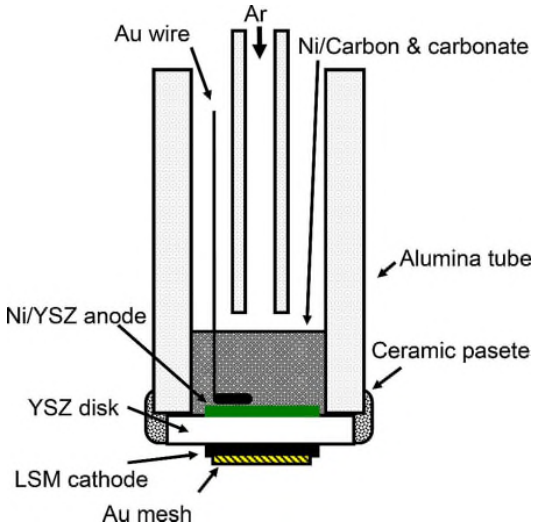

Figure 1. (Color online) Schematic diagram of the test cell.

* Electrochemical Society Active Member.
[c] Present address: Department of Organic and Polymeric Materials, Graduate School of Science and Engineering, Tokyo Institute of Technology, S5-20, Ookayama, Meguro-ku, Tokyo 152-8552, Japan.
[z] E-mail: jtsi@st-andrews.ac.uk

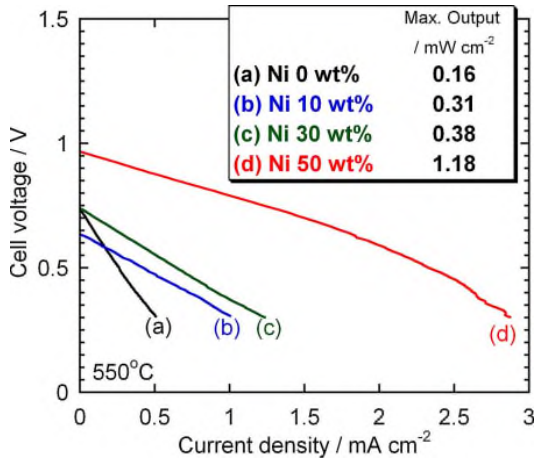

Figure 2. (Color online) *I-V* curves and maximum outputs of the HDCFC at 550°C with Ni/XC-72R as the fuel. Primary electrolyte: YSZ (2 mm thick), secondary electrolyte: Li_2CO_3/K_2CO_3 (62/38 mol %), anode: Ni/YSZ, and cathode: LSM/YSZ.

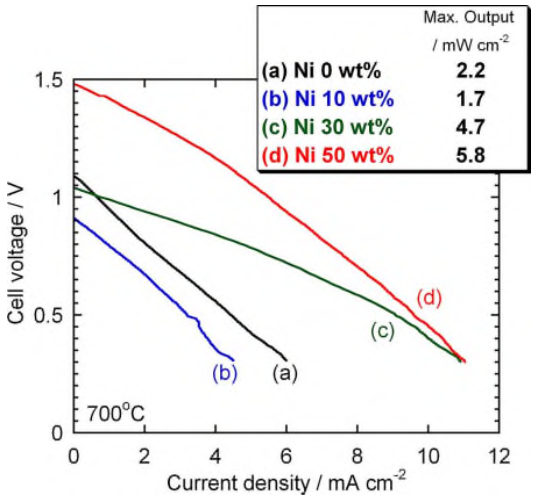

Figure 3. (Color online) *I-V* curves and maximum outputs of the HDCFC at 700°C with Ni/XC-72R as the fuel.

214.5 mg, which was equivalent to a height of about 3 cm of the powder mixture. Ar gas (100 mL min^{-1}) was fed to the anode compartment, and the cathode was exposed to static air.

Electrochemical measurements were carried out using a combined potentiostat and frequency response analyzer system (Solartron 1280B). The measurement was started at 550°C and then the temperature was raised stepwise to 900°C. All electrochemical measurements were started once a steady OCV was achieved, typically after 15–30 min, at each temperature. Current–voltage (*I-V*) curves were measured by a potential sweep at a scan rate of 1 mV s^{-1}.

TPD of the carbon/carbonate slurry.— Temperature-programmed decomposition (TPD) of the carbon/carbonate slurry in the HDCFC was carried out. A test cell with a mixture of carbon (with and without Ni) and carbonate was heated from room temperature to 700°C, at 4°C min^{-1}, monitoring the formation rates of gaseous products and OCV. Gaseous products were carried by the Ar purge and analyzed using an online gas chromatograph (Agilent Micro GC 3000) equipped with two capillary columns: MolSieve 5A PLOT with He carrier for CO detection and PLOT U with He carrier for CO_2 detection.

XRD analysis.— X-ray diffraction (XRD) patterns of the powders of Ni/XC-72R before and after the electrochemical measurements were measured in transmission mode using an X-ray diffractometer (STOE STADI-P) with Cu Kα radiation. The powder after the electrochemical measurement was rinsed with water and then filtered to remove the carbonate salt.

Results and Discussion

HDCFC performance with Ni/XC-72R.— Ni/XC-72R of 10, 30, and 50 wt % was studied to clarify how the addition of Ni improves the HDCFC performance. Figures 2 and 3 show the *I-V* curve of the HDCFCs at 550 and 700°C with Ni/XC-72R. The outputs of the HDCFC were calculated by multiplying the current densities with the cell voltages, and their maximum values are shown in the legend. At 550°C, the OCVs with 0, 10, and 30 wt % Ni samples were not very different, but the slope of the *I-V* curve was improved by the addition of Ni. The addition of 50 wt % of Ni drastically improved the OCV as well as the slope of the *I-V* curve. The trend in the HDCFC performance at 700°C was similar. The slope of the *I-V* curve was improved by adding 30 wt % of Ni, and the OCV was also improved by adding 50 wt % of Ni. The improvement in the slope of the *I-V* curves suggests that the kinetics of the carbon oxidation was improved by the addition of a Ni catalyst. The improvement in OCV suggests that the addition of a large amount of Ni affected the activities of reactants or products of the electrochemical oxidation in the carbon/carbonate slurry.

Figure 4 summarizes the OCVs and maximum outputs of the HDCFCs with the Ni/XC-72R (50 wt % Ni) and bare XC-72R (0 wt %) as functions of temperature. The OCVs were clearly improved at all tested temperatures by adding 50 wt % of Ni. Ni/XC-72R showed very high OCVs, approximately 1.5 V, at 700–900°C. The maximum outputs were also improved by the addition of Ni. The maximum outputs at 550, 600, 700, 800, and 900°C were improved by factors of 7.6, 5.8, 3.1, 2.5, and 1.4, respectively, by adding 50 wt % of Ni.

We reported very high OCVs close to 1.5 V at 550–700°C with bare XC-72R in an HDCFC.[14] Those high OCVs with bare XC-72R, however, can be obtained only after high temperature treatments at around 900°C, which enhance the decomposition of carbonate to

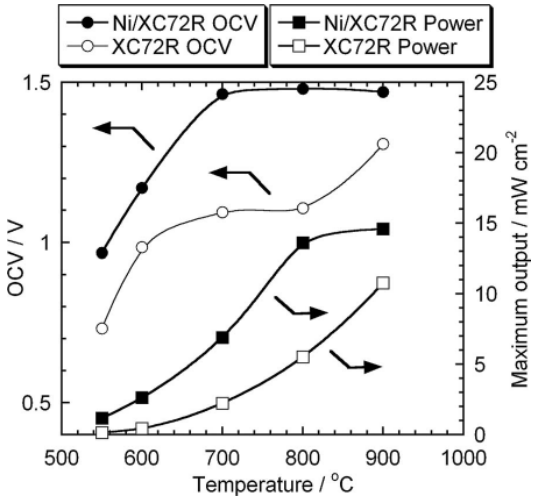

Figure 4. OCVs and maximum outputs of the HDCFC with Ni/XC-72R (50 wt %) as the fuel.

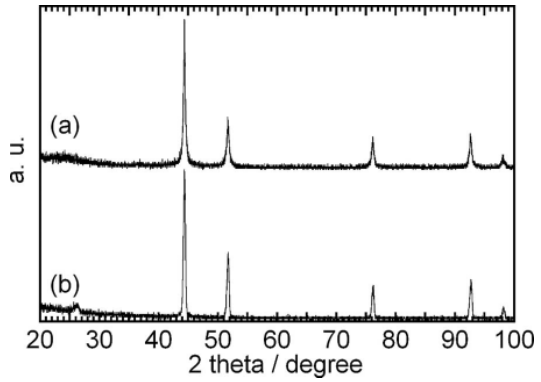

Figure 5. XRD pattern of the Ni/XC-72R (50 wt %) (a) as prepared and (b) after the electrochemical measurement.

yield Li_2O. The present data indicate that high OCVs and performance are obtained by utilizing Ni catalysts even without the high temperature treatments.

Ni particles before and after HDCFC testing.— Figure 5a shows the XRD pattern of Ni/XC-72R (50 wt %) as prepared. Strong peaks assigned to the Ni metal were observed.[15] The Scherrer equation was used to calculate the average crystallite size of the Ni metal

$$L = \frac{0.9\lambda}{B \cos \theta} \quad [1]$$

where L is the diameter of the crystallite, λ is the wavelength of the X-ray radiation (0.154 nm), θ is the Bragg angle, and B is the full width at half-maximum (fwhm) of the diffraction peak. The average crystallite size evaluated from the fwhm of the peak at 44.4° (2θ) was 26.9 nm. The sample after a series of HDCFC tests at 550–900°C, about 4 h in total, was also analyzed to clarify how the operating condition affects the state of Ni (Fig. 5b). No Ni species apart from the Ni metal were observed in the used samples. The average crystallite size from the fwhm was 20.3 nm, indicating that the dispersion of the Ni particles was sustained during the HDCFC test. These data suggest that the Ni nanoparticles are stable in the carbon/carbonate slurry under the operating condition of HDCFCs in this experimental time scale, although further long-term stability tests are required.

TPD of the carbon/carbonate slurry.— The TPD of the carbon/carbonate slurry is suitable for discussing how the Ni catalyst affects the activities of the chemical species in the carbon/carbonate slurry at open-circuit condition. The TPD of the carbon/carbonate slurry was carried out by heating the carbon/carbonate slurry in the test cell. Figure 6 shows the formation rates of CO and CO_2, and OCV while heating the test cell with the Ni/XC-72R and XC-72R. At the early stage of the TPD up to 300°C, any gaseous products were not observed, except for CO_2 from bare XC-72R. This CO_2 probably derives from the surface functionalities of the carbon black. It is reasonable that this kind of CO_2 was not observed from Ni/XC-72R as it had been treated at 400°C during the catalyst preparation. When the cell temperature reached around 300°C, the formation of CO_2 started in both samples. This CO_2 would be produced by the decomposition of CO_3^{2-}

$$CO_3^{2-} \rightarrow CO_2 + O^{2-} \quad [2]$$

As the cell temperature increased, the formation rates of CO_2 decreased and the formation of CO started instead. CO can be produced by the reverse Boudouard reaction

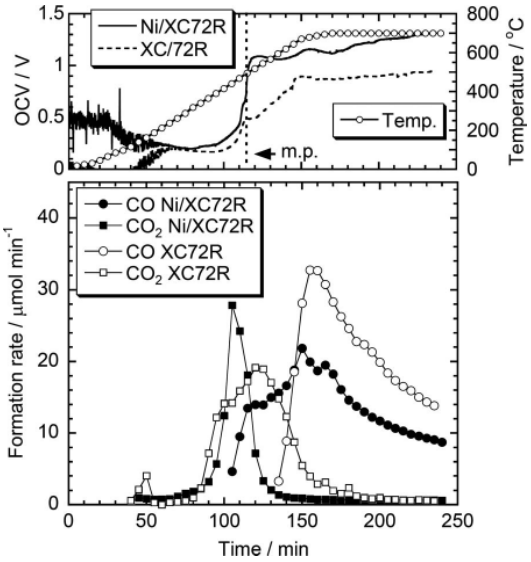

Figure 6. TPD of the slurry of Ni/XC-72R and carbonate monitoring the OCV.

$$C + CO_2 \rightarrow 2CO \quad [3]$$

This observed trend in the selectivity of CO to CO_2 corresponds to the thermodynamic prediction for equilibrium of Eq. 3.[16] The main difference in the gaseous products between two samples was the temperature where CO appears: 440°C with Ni/XC-72R and 600°C with XC-72R. This suggests that the Ni catalyst enhances the reverse Boudouard reaction (Eq. 3) in the carbon/carbonate slurry.[17,18]

The OCVs with both samples were quite low at the early stage, and they increased when the cell temperature reached a value close to the melting point of the eutectic mixture (488°C). The OCV with Ni/XC-72R rapidly increased up to 1.1 V, and then gradually increased to 1.31 V. In contrast, the OCV with XC-72R gradually increased, but reached only 0.94 V.

High OCV with Ni/XC-72R.— As shown above, Ni/XC-72R shows extremely high OCVs over 700°C compared to bare XC-72R. These values are much higher than the theoretical standard potentials for carbon oxidation to CO_2

$$C + O_2 \rightarrow CO_2 \quad (E^\circ = 1.03 \text{ V at } 700°C) \quad [4]$$

To explain the very high OCVs, it is necessary to consider two types of mediators in the HDCFC system. Herein the reaction schemes and the thermodynamics involving these mediators are discussed on the basis of the thermodynamic calculation[16] at 700°C, where the effect of Ni is the most significant.

One possible mediator is the CO_3^{2-}/O^{2-} mediator, as discussed in our previous work.[14] As shown in the TPD data, CO_3^{2-} thermally decomposes to CO_2 and O^{2-} in these experimental conditions. While the electrochemical reaction produces CO_2 in the HDCFC, O^{2-} can trap the produced CO_2 to form CO_3^{2-} and keep the activity of CO_2 in the carbon/carbonate slurry quite low. The low activity of CO_2 increases the Nernst potential of Eq. 4 by 0.20 V. Considering the effect of the recombination on the Nernst potential is the same thing as calculating the reaction Gibbs function of Eq. 5 (Ref. 14)

$$C + O_2 + Li_2O \rightarrow Li_2CO_3 \quad (E^\circ = 1.22 \text{ V at } 700°C) \quad [5]$$

Li^+ is herein considered as the counter cation to simplify the issue. This reaction has a higher standard potential than that of Eq. 4, because the decomposition of CO_3^{2-} is an endothermic reaction. This mediator would work continuously if the recombination of CO_2 and

O^{2-} and the formation of O^{2-} by the decomposition can be balanced. The effect of this mediator is stronger as the decomposition CO_3^{2-} becomes faster.

The TPD results suggest that the amount of decomposed carbonate was not affected by the Ni catalyst: 1.6 and 2.1 mmol, respectively, with Ni/XC-72R and XC-72R, which were evaluated by integrating the formation rates of CO and CO_2. Thus there may be some contribution of the CO_3^{2-}/O^{2-} mediator to the OCVs with the HDCFCs in this study, but the degree of the contribution is similar between the HDCFCs with Ni/XC-72R and XC-72R.

The other possible mediator is the CO_2/CO mediator. If the reverse Boudouard reaction (Eq. 3) is fast enough, the electrochemical reaction on the anode can start from CO as well as from C

$$2CO + O_2 \rightarrow 2CO_2 \quad (E^\circ = 1.03 \text{ V at } 700^\circ C) \qquad [6]$$

Although the Nernst potential of Eq. 6 itself is not different from that of Eq. 4, the effect of the recombination of CO_2 and O^{2-} significantly increases the Nernst potential

$$2CO + O^2 + 2Li_2O \rightarrow 2Li_2CO_3 \quad (E^\circ = 1.42 \text{ V at } 700^\circ C) \qquad [7]$$

This calculation suggests that the oxidation of CO shows a higher OCV than that of C if the CO_3^{2-}/O^{2-} mediator is working.

The measured OCV with Ni/XC-72R is close to the Nernst potential of Eq. 7. Besides, the TPD result suggests that the Ni catalyst enhances the reverse Boudouard reaction under these experimental conditions. The high OCV with the Ni/XC-72R was probably derived from the oxidation of CO under the mediation by the CO_3^{2-}/O^{2-} system.

Figure 7 summarizes the thermodynamics at 700°C with several patterns of reaction schemes. Theoretical heat balance Q was calculated from the enthalpy change (ΔH) of the nonelectrochemical processes and the entropy change (ΔS) of electrochemical processes. The hydrogen fuel cells (Fig. 7a) electrochemically oxidize H_2 to H_2O, and the reaction Gibbs function ($\Delta G^\circ = -388.4$ kJ mol^{-1}) is converted to electric power. The heat equivalent to $-T\Delta S$ (106.7 kJ mol^{-1}) is exhausted; therefore the system is exothermic. Normal DCFCs without any following reaction (Fig. 7b) electrochemically oxidize carbon to CO_2. The standard potential (E°) of this system is similar to that in the hydrogen fuel cells, but the entropy change is quite small. In the HDCFCs with the CO_3^{2-}/O^{2-} mediator (Fig. 7c), the CO_2 produced on the electrochemically active sites is trapped by O^{2-} to form CO_3^{2-}; therefore the activity of CO_2 around the electrochemically active sites is quite low. O^{2-} can be regenerated in the bulk of the carbon/carbonate slurry, as the decomposition of CO_3^{2-} is not an electrochemical reaction. In the HDCFCs with both CO_3^{2-}/O^{2-} and CO_2/CO mediators (Fig. 7d), CO_2 is converted to CO in the reverse Boudouard reaction in the bulk of the carbon/carbonate slurry, and the actual electrochemical reaction starts from CO. As the decomposition of CO_3^{2-} and the reverse Boudouard reaction are both endothermic reactions, the electrochemical reaction Eq. 7 can release a large volume of Gibbs free energy, although the system becomes endothermic.

Figure 7c and d suggests that nonelectrochemical endothermic reactions increase the Nernst potential of the electrochemical reactions. Fuel cell operation around OCV in such systems is not practical because the system is not thermally sustainable. In practical fuel cells, however, the operating voltage must be lower than OCV because of the ohmic loss and overpotential. These concepts suggest that very efficient energy conversion is achievable by operating HDCFCs with a certain volume of current around the Nernst potential of the carbon oxidation (1.03 V at 700°C), where the heat emission by the electrochemical processes and the heat adsorption by the nonelectrochemical processes are balanced.

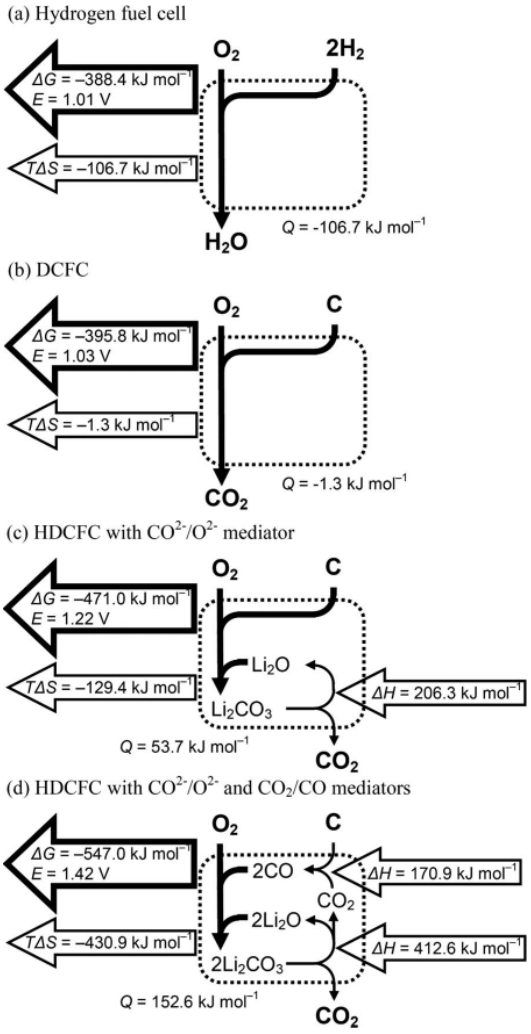

Figure 7. Schematic diagram of the thermodynamics for the fuel cells under various conditions. Bold arrows: electrochemical processes, normal arrows: nonelectrochemical processes.

Conclusions

Ni/XC-72R was tested as a fuel for HDCFCs with solid oxide and molten carbonate binary electrolyte. The OCV and maximum output were improved by adding Ni metal as a catalyst (1.5 V at 700–900°C). The TPD data suggest that the Ni catalysts enhance the reverse Boudouard reaction. CO produced by the reverse Boudouard reaction is electrochemically oxidized to CO_2 followed by the recombination of CO_2 and O^{2-}. The proposed reaction scheme suggests that very efficient energy conversion is possible with HDCFCs.

The present results suggest that the performance of the HDCFC is highly dependent on the anode kinetics. Minimizing the loading of Ni and optimizing the catalyst preparation are quite important to maximize the total energy conversion efficiency of the HDCFC, although Ni catalysts on the carbon fuel is not the only way to improve the anode kinetics. Further investigation to improve the anode kinetics and to obtain better durability is required.

Acknowledgments

The authors thank Scottish Enterprise and EPSRC for funding, Robert Marshall Associates for support, and Sneh L. Jain for valuable discussion and assistance.

University of St. Andrews assisted in meeting the publication costs of this article.

References

1. D. Cao, Y. Sun, and G. Wang, *J. Power Sources*, **167**, 250 (2007).
2. K. Pointon, B. Lakeman, J. Irvine, J. Bradley, and S. Jain, *J. Power Sources*, **162**, 750 (2006).
3. S. Zecevic, E. M. Patton, and P. Parharni, *Carbon*, **42**, 1983 (2004).
4. W. W. Jacques, *Harper's Magazine*, **94**, 144 (1896).
5. D. G. Vutetakis, D. R. Skidmore, and H. J. Byker, *J. Electrochem. Soc.*, **134**, 3027 (1987).
6. W. H. A. Peelen, M. Olivry, S. F. Au, J. D. Fehribach, and K. Hemmes, *J. Appl. Electrochem.*, **30**, 1389 (2000).
7. N. J. Cherepy, R. Krueger, K. J. Fiet, A. F. Jankowski, and J. F. Cooper, *J. Electrochem. Soc.*, **152**, A80 (2005).
8. N. Nakagawa and M. Ishida, *Ind. Eng. Chem. Res.*, **27**, 1181 (1988).
9. T. M. Gur and R. A. Huggins, *J. Electrochem. Soc.*, **139**, L95 (1992).
10. T. Horita, N. Sakai, T. Kawada, H. Yokokawa, and M. Dokiya, *J. Electrochem. Soc.*, **142**, 2621 (1995).
11. M. Ihara and S. Hasegawa, *J. Electrochem. Soc.*, **153**, A1544 (2006).
12. A. S. Liplin, I. I. Balachov, L. H. Dubois, A. Sanjurjo, M. C. McKubre, S. Crouch-Baker, M. D. Hornbostel, and F. L. Tanzella, U.S. Pat. 20060019132 (2006).
13. S. L. Jain, J. B. Lakeman, K. D. Pointon, and J. T. S. Irvine, *J. Fuel Cell Sci. Technol.*, **4**, 280 (2007).
14. Y. Nabae, K. D. Pointon, and J. T. S. Irvine, *Energy Environ. Sci.*, **1**, 148 (2008).
15. JCPDF Card no. 4-850.
16. A. Ronie, Outokumpu HSC Chemistry 5.1, 2002.
17. D. W. McKee, *Chem. Phys. Carbon*, **16**, 1 (1981).
18. S. Takenaka, Y. Tomikubo, E. Kato, and K. Otsuka, *Fuel*, **83**, 47 (2004).